Adsorption of single metallic atoms on self-assembled molecular domain of terephthalic acid

Hao Tang, Corentin Durand, Roland Coratger

Version of Record: https://www.sciencedirect.com/science/article/pii/S2468023021002479
Manuscript_72d849fd2b062d3377423a02affb8de2

Adsorption of single metallic atoms on self-assembled molecular domain of terephthalic acid

Hao Tang, Corentin Durand, Roland Coratger

SINANO Group, CEMES/CNRS, 29 rue J. Marvig, 31055 Toulouse, France and Université Paul Sabatier, 118 route de Narbonne, 31000 Toulouse.
Tel: 05 62 25 78 99 E-mail: coratger@cemes.fr

Abstract

Cobalt and gold atoms have been deposited on self-assembled molecular domains of terephthalic acid and are studied using low temperature scanning tunneling microscopy and DFT calculations. These two types of atoms present different adsorption properties as well as peculiar electronic structures. Co atoms are firmly adsorbed on the molecules while Au is highly dependent of the presence of diffusing hydrogen atoms. These latter can also favour the possible desorption of the adatoms or change their adsorption site depending on the presence of defective molecules. The results open the way to new investigations concerning the use of single atoms or molecules for chemistry at the subnanometer scale.

Keywords: Scanning tunneling microscopy, DFT, single atom, molecular self-assembly, adsorption, terephthalic acid.

1. INTRODUCTION

During the last decades, a considerable number of experimental and theoretical works has been published concerning adsorption of molecules on solid surfaces. These investigations are mainly motivated by the development of molecular electronics [1, 2] and concern the behaviour of molecules either self assembled in well organized domains [3, 4, 5] or as single objects adsorbed on a solid surface [6, 7, 8]. In large self-assemblies, the interactions between molecules considerably weaken the individual role of each molecule. However, these domains are rather solid especially if one considers possible metal-ligand interactions [9, 10, 11] or covalently bounded systems [12, 13, 14, 15, 16]. This relative robustness makes these systems good candidates for technological applications. The problem for single atoms or molecules is different. They certainly constitute the best model systems from a physical and chemical point of view (the interactions with the surrounding objects are then minimized) but their high mobility implies that the observations and manipulations are performed at very low temperatures [17]. For example, using the high resolution of near field techniques such as scanning tunneling microscopy (STM) and atomic force microscopy (AFM) it is possible to observe and manipulate single atoms or molecules with the constraint of working at liquid helium temperature [18, 19, 20].

Another possibility is to use self organized domains as host porous structures in which the single adsorbates (up to now essentially molecules) would be engaged [21, 22, 23]. However, the concept of porous host structure generally used to trap molecules can perfectly be expanded to single atoms that would be adsorbed on a molecular self-assembly. Depending on the molecular symmetries, one is able to predict the shape, periodicity and symmetry of the host lattice. Thus, this offers the possibility to study single objects embedded in self organized synthons. To accommodate large molecules such as C_{60} for example, the pore size as to be large enough [22] but for single atoms, this constraint is less important and most of the molecular lattices can be good candidates.

Among them, self assemblies of terephthalic acid (TPA) are a typical example of possible host structure for adatoms. Indeed, self-assembled domains of TPA deposited on different metallic and semiconducting substrates have been largely studied [24, 25, 26] and these studies have demonstrated that the formed structure are rather stable, at least when they are kept at low temperature. When adatoms are co-evaporated with the molecules or on reactive substrates, metal-carboxylates compounds are formed [27]. On low reactive Ag(111) surfaces, deprotonation of these molecules occurs at ambient temperature and leads to characteristic dark defects on the STM images. The formation of these dark contrasts due to deprotonation of TPA has been previously demonstrated on other substrates such as Cu(100) [28, 29] and on Ag(111) even at the single molecule level using localized voltage pulses and DFT calculations [30]. Despite these defects, the networks remain stable and their inner structure is always maintained by hydrogen bonding between COOH groups.

In this paper, self-assemblies of TPA molecules have been used as host lattices for adsorption of single cobalt and gold atoms deposited at liquid nitrogen temperature. These adatoms have been chosen because they can be easily evaporated at relative low temperature (less than 1500 °C for Co) from a metallic wire heated for example by a W filament. Moreover, these species have been largely studied by near field techniques and their behaviour is well referenced. Interestingly, these atoms are bounded to the underlying molecules and can be stable depending of their adsorption site. The adatoms have been observed and characterized with a high stability by STM and scan-

ning tunneling spectroscopy (STS). These observations supported by DFT calculations demonstrate that the two atoms present different adsorption sites and different electronic properties once adsorbed. While Co atoms highlight a unique adsorption site, Au adatoms exhibit different possibilities due to their reactivity with diffusing H atoms. This includes the possibility to remove the Au adatoms or to change their apparent height during the tip scan.

2. EXPERIMENTAL DETAILS

STM experiments have been performed at liquid nitrogen temperature (T = 77.8 K) on a commercial STM (LT Omicron) working with a base pressure of $2x10^{-11}$ mbar. The terephthalic acid (TPA) molecules were evaporated on a Ag(111) substrate from a quartz crucible heated by a W wire 0.25 mm in diameter. This evaporator was first pumped by a turbo molecular pump during at least 12h before deposition. Evaporations on the substrate held at room temperature were performed in the preparation chamber and the observed deposition rate was about half a monolayer per minute for a electric power of 0.3 W applied to the crucible. The Ag(111) crystal was cleaned by repeated Ar^+ bombardment cycles at E = 600 eV followed by annealing at 750 K for 45 minutes. Afterwards, the substrate was transferred to the STM chamber to be cooled down at the desired temperature. Evaporations of adatoms (Co and Au) have also been conducted on a cold substrate. For this, the sample consisting of the Ag(111) substrate covered with TPA self assemblies was removed from the STM head and placed 5 centimeters above the crucible to reach the desired evaporation rate. As the aim is to deposit only single atoms, the deposition was performed during less than one minute and the sample was immediately reintroduced on the STM head to be cooled down. The whole process took about a few tens of seconds and it is estimated that the sample temperature never exceeded 120 K. The adatoms were evaporated from small Au and Co wires 0.15 mm in diameter heated by Joule effect and placed on specially adapted sample plates that can be easily transferred throughout the different UHV chambers. STM tips made of tungsten wires 0.2 mm in diameter were prepared by electrochemical etching and cleaned in UHV using direct current heating. The bias voltage indicated in the text was always applied to the sample. Scanning tunneling spectroscopy (STS) experiments are performed with a lock-in amplifier working at 413 Hz and with a bias modulation of 15 mV.

3. THEORETICAL METHODS

The density functional theory (DFT) calculations were carried out by using the Vienna Ab-initio Simulation Package (VASP, version 5.4.4) [31], [32]. During these calculations, the projector augmented wave (PAW) method was applied in a plane wave basis set [33] to describe the valence electron - core interaction. The Perdew-Beck-Eneker (PBE) functionnal was used for the exchange-correlation interaction in the frame of the generalized gradient approximation (GGA) [34]. The van der Waals (vdW) dispersion interaction was included semi-empirically according to our modified version of the DFT-D2 method proposed by Grimme [35]. The kinetic energy cut-off was set to 440 eV, which gives an optimized lattice parameter of 4.162 Å for the fcc Ag bulk. The self-consistent electronic convergence criterion was set to 10^{-7} eV and the geometrical relaxation was considered to be converged when the forces on each unfixed atom was lower than 0.02 eV/Å. The Ag(111) substrate was simulated by a slab composed by 4 atomic layers with a lateral dimension of 11.77 x 20.61 $Å^2$. The self-assembled monolayer was simulated by four TPA molecules oriented along the $\langle 11\overline{2}\rangle$ direction inside a (2x2) unit-cell. The Brillouin zone was sampled with the gamma point in the reciprocal space for the geometric optimization calculations and a 3x3 in-plan Monkhorst-Pack grid [36] was used to obtain the electronic structures. The vacuum was set to about 17 Å (above the molecules, and about 20 Å from the Ag surface) in order to minimize the interaction between neighbour super-cells in the z direction. The dipole in this z direction was also corrected to avoid the artificial interaction between interface dipoles in periodic cells.

For a complete description of the presented structures, the activation barriers between the different conformations have to be calculated. These latter are estimated by the Climbing Image Nudged Elastic Band (CI-NEB) method as implemented by the Henkelman group (at UT Austin) [37, 38]. With this method, the minimum energy reaction path is identified, by optimizing the forces perpendicular to this path to be lower than 0.5 eV/Å on each of equally separated intermediate images. Deliberately, calculations have been limited to this rough transition state because the more precise Dimer method [39, 40] requires too much computation resources.

4. RESULTS AND DISCUSSION

4.1. Main characteristics of the TPA self-assembly

The TPA molecules deposited on low reactive Ag(111) surfaces form self assemblies as presented in Fig. 1a. In these structures, TPA form bands in which the molecules are coupled head to tail through linear [O-H..O] bonds (Fig. 1b). Theses bands are formed by 1D molecular chains separated by 0.68 nm. The Bravais lattice is oblique (γ=102°±3°) and the distance between nearest neighbours is about 0.8 nm (Fig. 1c). These bands are randomly oriented with respect to the dense <110> or <211>-type directions of the metallic substrate and can be interconnected as suggested in the upper part of Fig. 1a.

These structures are stable even at ambient temperature but after several hours or after a soft annealing of the layer at about 100°C, a partial deprotonation of the molecules may occur [30]. This deprotonation can be also induced by the STM tip when a voltage pulse above 1.2 V is applied on one of the [O-H..O] bonds. Thus, when the self-assemblies are kept at liquid nitrogen temperature and when low bias voltages are used for STM imaging, the molecules and then the self assembled domains remain intact. Another striking characteristic of these structures results from their interaction with the 2D electron gas of the

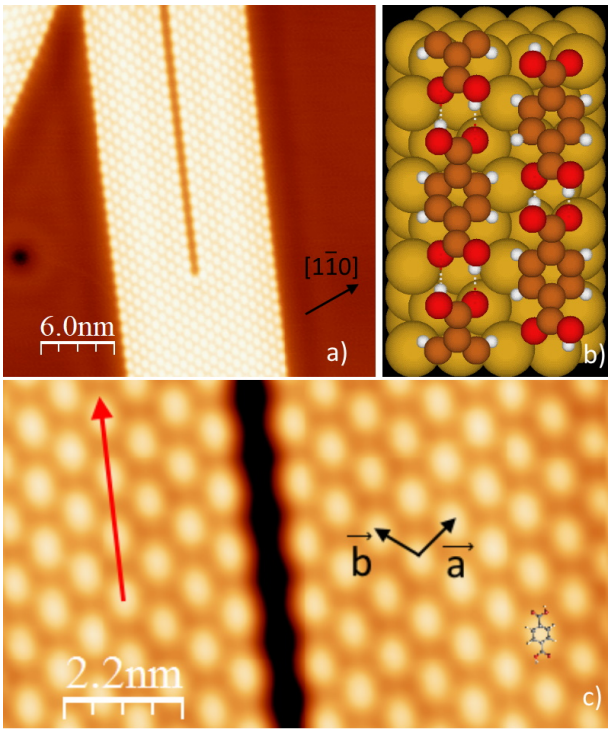

Figure 1: a) STM image (30x30 nm^2) of the TPA rows self-assembled in bands on the Ag(111) surface (V=100 mV, I=5 pA, T=77K). b) Details of the molecular structure on Ag(111) as deduced from DFT calculations. The largest balls are used for the Ag atoms. White, brown and red atoms represent the hydrogen, carbon and oxygen atoms respectively. c) Zoom of (a) showing the network of molecules and the surface Bravais lattice (V=75 mV, I=5 pA, T=77K). The angle between the two vectors is 102°±3°. The red arrow shows the [11] direction corresponding to a 1D TPA chain connected by hydrogen bonds.

substrate. Indeed, the characteristic surface state of Ag(111) located originally 70 meV below the Fermi level is shifted in energy when this latter is covered with the TPA network and is measured 50 meV above E_F.

4.2. Evaporation of Co atoms

These molecular self assemblies are used as host lattice for Co atoms deposited at low temperature. This process has to be relatively fast to avoid sample heating and with very low fluxes to avoid large coverage rates. After cooling down at 77K, the sample is scanned using the same parameters than those previously used for TPA/Ag(111), *i.e.* typically a few hundreds of mV up to one volt for the bias voltage and a few tens of picoamperes for the tunneling current. Fig. 2 shows a TPA layer after such a deposit. The Co adatoms appears as small bumps essentially on the edges of the domain. Thus, those deposited directly on the substrate diffuse at this temperature and can reach the molecular network where they form quasi-linear chains of adatoms (for more precise observations, a small scale STM image is presented Fig. 1 in Supplementary Informations). Co atoms can be also adsorbed on a second ML (as shown by the red arrow in the lower right part of Fig. 2). Their apparent size is identical whatever the number of molecular layers below. One can also note that no atoms are adsorbed directly on the Ag(111) surface or against a molecular layer which reinforces the idea of surface diffusion before final adsorption.

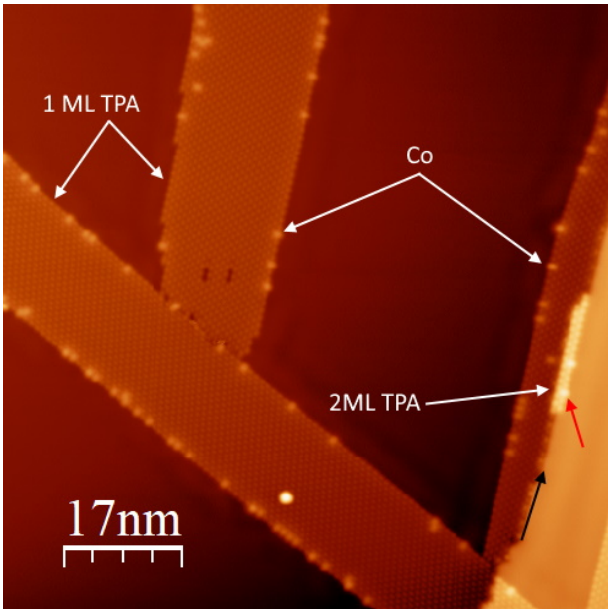

Figure 2: Large scale STM image (82x82 nm^2) of the surface after deposition of Co atoms on TPA/Ag(111). The black arrow indicates a monoatomic Ag step separating two (111) terraces. The red one indicates a second layer of TPA (V=-300mV, I=5 pA, T=77K).

A close inspection of the TPA network around a Co atom shows that this latter is exactly adsorbed on top of the benzene ring of the underlying molecule (Fig. 3). This is also the case for the Co atoms adsorbed on the edges of the molecular domains. The Co atoms exhibit an apparent height of typically 1.5 Å with respect to the TPA layer in these tunneling conditions. This lateral size is consistent with the previous papers concerning single Co atoms in which it appears that these dimensions are substantially larger than the real atomic size, a phenomenon well-known in STM imaging [41]. However, the apparent corrugation is slightly higher than usually observed on metallic surfaces. This can be attributed to the small decoupling character of the molecular layer leading to an electron density on each Co atom higher than when these latter are deposited directly on the metallic substrate.

Because of this ability to diffuse, Co is able to form small chains of atoms along the molecular domain edges with an interatomic distance equal to the intermolecular distance along the TPA chains (*i.e.*, 1.1 nm). Thus, these sites seem to be particularly reactive since most of the Co atoms adsorb here after diffusion on the Ag terraces or on the self-assemblies. Once adsorbed, these atoms are stable at liquid nitrogen temperature. Note also that no Co atom is adsorded directly on the substrate. Thus, when a larger amount of Co atoms are deposited, these latter produce small clusters on TPA but without any crystallographic structure.

The electronic properties of these adatoms have been also studied by STS (see Fig. 4). On the substrate, the STS spectrum shows the characteristic onset due to the 2D electronic surface

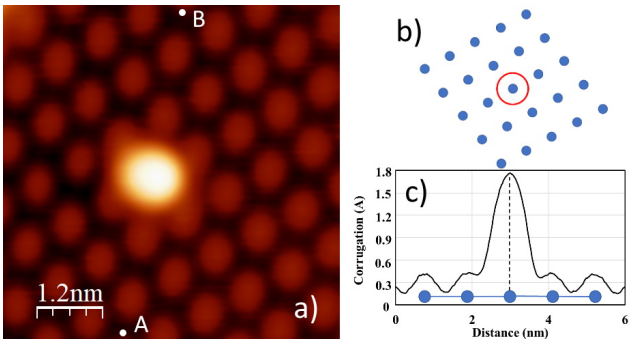

Figure 3: a) STM image of the adsorption site of a single Co atom on a TPA network. b) Schema of the molecules (blue balls) surrounding the metallic atom represented by the red circle. c) Cross section between points A and B. The highest corrugation is highlighted by the vertical dashed line (V=-400mV, I=5 pA, T=77K).

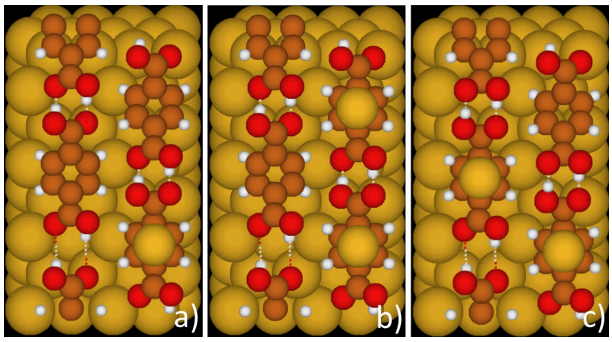

Figure 5: (a) DFT calculations showing the structure of a Co atom adsorbed on a TPA monolayer. b) Surface after adsorption of two Co atoms along the same TPA chain and separated by 9.74 Å. c) Structure of two Co atoms adsorbed on two nearest TPA neighbours. In this case, the Co interatomic distance is 7.85 Å.

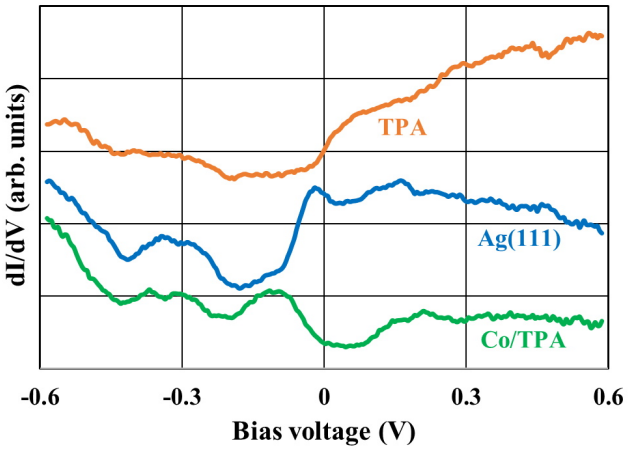

Figure 4: Scanning tunneling spectroscopy of the Ag(111) substrate (blue curve), the TPA layer (brown curve) and a cobalt atom lying on a TPA (V=600 mV, I=100 pA, f=413 Hz, ΔV=15 mV , T=77K).

state at 70 meV below the Fermi level. On the molecular layer, this surface state is shifted because of the interaction of the electron gas with the self assembly which forms an interface state confined to the molecule/metal interface [44]. The STS curve shows that this interface state is now around or slightly above E_F. This upwards energy shift is found to depend on the size of the molecular assembly and for the largest domains (for example a complete monolayer), this offset reaches 150 meV with respect to the Ag(111) surface state. On the adsorbed Co adatom, the behavior around the Fermi level is different. A characteristic peak at 110 meV below E_F appears and the contribution of the interface electronic states disappears. The same characteristic can be also observed for dimers or adatoms adsorbed at the edges of the domains.

4.3. Calculations for Co atoms on TPA

Starting from the (2x2) TPA monolayer adsorbed on Ag(111), the cobalt atom spontaneously adsorbs on the position localized above the center of the benzene core of TPA (Fig. 5). The adsorption energy is -4.083 eV, with a vertical distance of 1.481 Å to the benzene ring. The vdW contribution is -0.232 eV and thus the chemical binding energy is -3.851 eV. The magnetic moment of Co is 1 μ_B. The Fermi energy is slightly increased to -0.87 eV (compared to -0.95 eV for a TPA self-assembly on Ag(111)). The work function has decreased from 3.85 eV to 3.62 eV. Finally, 0.96 electron is transferred from the Ag substrate to the TPA monolayer. This latter has got a net gain of 1.5 electrons and the Co atom has lost 0.54 electron.

When two Co atoms are adsorbed on the benzenes of adjacent TPA molecules (separated by about 9.74 Å along the $\langle 11\bar{2} \rangle$ direction) as for dimers in the edges of the domain presented in Fig. 2, the adsorption energy per Co atom is -3.994 eV with the spins oriented in parallel and this energy is -3.840 eV per atom when the spins are anti-parallel. When Co atoms are adsorbed on the nearest TPA neighbours (7.85 Å as for dimers in middle of the domain presented in Fig. 2), the adsorption energy per atom is -4.008 eV with their spins in parallel, and -3.855 eV for anti-parallel spins. The low energy difference between these two configurations for dimers suggest that no configuration is preferred. Experimentally, the first configuration is essentially observed on the molecules lying at the edges of the domains while the second is almost exclusively observed in the middle of the molecular assemblies. However, the difference in adsorption energy suggests that whatever the configuration (in the same TPA chain or on the two nearest molecules), two Co atoms adsorb in a parallel spin configuration.

The projected density of states have been also calculated and the results are shown in Fig. 6. Important differences with the density of states of the molecular layer appear when a Co atom is adsorbed. These differences mainly concern the occupied electronic states, *i.e.* below the Fermi level. Particularly, significant contributions 180 meV and 810 meV below E_F due to Co adsorption are highlighted. The contribution nearest the Fermi level is close from the peak experimentally observed 110 meV below E_F. Below the Fermi level, this contribution is also highlighted in Fig. 2 of Supplementary Informations in which the difference between the experimental spectra obtained

on Co/TPA and directly on the TPA layer are presented. Concerning the feature at -810 meV, it cannot be experimentally detected because of the instabilities that appear on adsorbed atoms while scanning at such "high" voltages. However, it is observed that the differential conductance deduced from the dI/dV curves increases ~500 meV below E_F, an increase which is larger than the one simply produced by the Ag substrate in this energy range (Fig. 4). Then, this feature can be related to the rise in the PDOS due to the Co contribution.

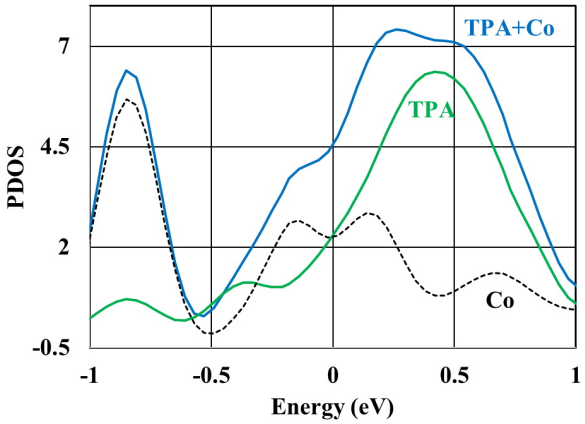

Figure 6: DFT Calculations of the Projected Density Of States (PDOS) for the TPA layer (green curve) and the Co atom adsorbed on the benzene ring of a TPA as in Fig. 5a (blue curve). The dashed curve gives the contribution of the cobalt atom.

4.4. *Evaporation of Au atoms*

The same experiments have been performed with gold atoms and an example of the surface after Au evaporation on a TPA layer is shown in Fig. 7.

This deposition results in the apparition of the single metallic adatoms as small bumps randomly distributed over the surface. These latter are then stable at liquid nitrogen temperature. Most of them are located on the TPA structures (see the longest white arrow in the lower part) and only a few are adsorbed directly on the metallic substrate. One of them is pointed by the shortest white arrow in the lower part of the STM image. In spite of the low temperature, these Au atoms have diffused on the surface and are anchored to the molecular structure. A gold atom is also adsorbed on a second layer (2ML) of TPA in the central right part of the image (red arrow). A first observation suggests that these atoms exhibit almost the same shape whatever their adsorption site. One can simply note that their apparent diameter is slightly larger when the atom is adsorb on the molecular layer but do not depend on the number of TPA layers since the single atom adsorbed on the second ML presents the same size than those located on 1 ML TPA assembly. Contrary to Co adatoms, Au adatoms are able to stay on the metallic substrate close to the TPA assemblies and but when the coverage increases, these adatoms diffuse and produce small triangular or hexagonal Au clusters against the TPA networks, typical of the (111) growth of these two metals [42].

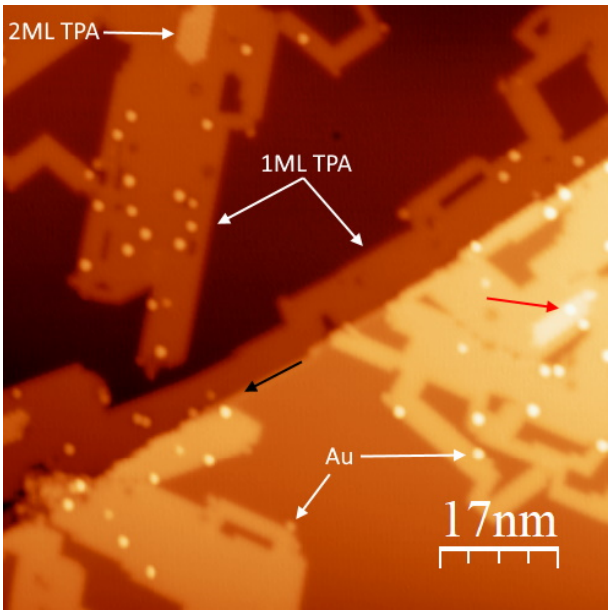

Figure 7: Large scale STM image (82x82 nm^2) of self-assembled TPA domains after evaporation of Au atoms. The black arrow indicates a monoatomic Ag step separating two (111) terraces (V=600 mV, I=2 pA, T=77K, t_{evap}=10 s).

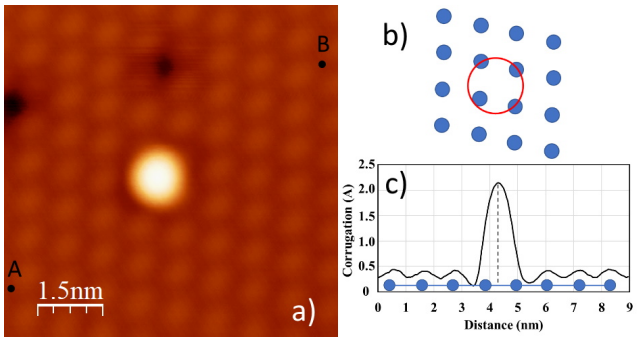

Figure 8: a) Small scale STM image showing the position of a Au atom on the TPA self-assembly. b) This schema shows the molecule positions surrounding the adatom (balls in blue) and the position of the largest corrugation due to the metallic atom (red circle). c) Cross section taken from the STM image between points A and B. The molecular positions are in blue and the position of the highest corrugation is indicated by the vertical dashed line (V=600mV, I=2 pA, T=77K).

Small scale images have been acquired to study the most frequently observed position of the Au atoms with respect to the TPA lattice. Fig. 8a presents a close view of an Au atom adsorbed on the TPA monolayer. The two defects located in the upper part result for the deprotonation of two molecules as usually observed on this type of self-assembly. The small schema in the upper right part (Fig. 8b) has been deduced from the experimental image and gives the positions of the molecules in blue while the red circle determines the position of the metallic adatom. The curve presented in Fig. 8c is a cross section conducted from point A to point B along the row. The vertical dashed line locates the maximum of the apparent height. This corrugation is relatively large (about 2 Å) and comparable to

what is observed for single Au atoms adsorbed on thin insulating layers of NaCl [43, 44] and 0.5 Å larger than for Co. With this difference in corrugation comes a modification of the adsorption site. Indeed, the Au atom is adsorbed between two molecules along a row and not on the benzene ring. However, its position is not exactly in the center of the four surrounding molecules but is slightly displaced towards one of the molecule of the row. This small shift is about 1.6 Å in Fig. 8, indicating that the adsorption position is 0.38 nm from the center of the benzene ring of the nearest molecule along the 1D chain. Several gold atoms can be adsorbed side by side as presented in Fig. 3 of Supplementary Informations. In this case, their adsorption site is the same and their interatomic distance is then related to the molecular network (about 0.85 nm along one of the Bravais direction).

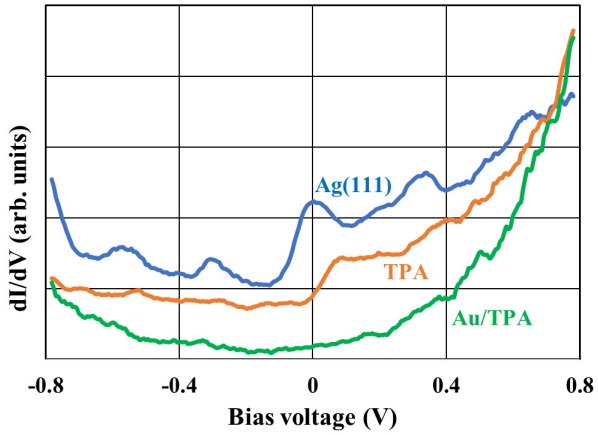

Figure 9: Scanning tunneling spectroscopy performed on the Ag(111) substrate (blue curve), the TPA assembly (orange curve) and a single Au adatom (green curve). The spectra have been vertically shifted for clarity (V=800 mV, I=100 pA, f=413 Hz, ΔV=15 mV , T=77K).

The electronic properties of these adatoms have been also studied by STS and the results are reported in Fig.9. The spectra performed on the substrate and on the TPA self-assembly exactly present the same characteristic than those previously shown in Fig. 4. The energy shift observed is slightly more important in this case. As explained before, this results from the lateral size of the TPA domain which directly influences the confinement of the interface state and then, its energy position with respect to E_F. The narrower the self assembly, the less the peak shifts with respect to the Ag(111) surface state. On the gold adatom, the characteristic interface state at 70 meV below the Fermi level disappears and a smooth quasi-parabolic variation of the electronic density is observed in this energy range. Note that the same spectrum is observed for stable Au adatoms adsorbed on second layers of TPA or when they directly lay on the substrate. This indicates that these atoms strongly change the electronic properties at the interface over an area of several angstroms around them and that the role of the TPA molecules is weak with respect to the link between the single Au atoms and the underlying substrate. As compared to the Co atoms, there is no specific electronic state below E_F.

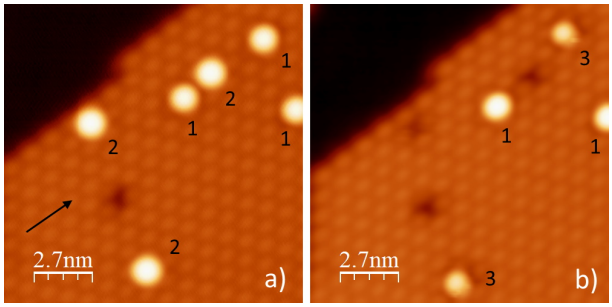

Figure 10: a) STM image of six Au atoms adsorbed on TPA. A defect due to deprotonation of a molecule can be observed near the center. The black arrow gives the direction of the TPA chain. b) Same area after removing two Au atoms and contrast modifications for two others. The removal of the two adatoms induces the creation of defects due to deprotonation in the layer. The numbers 1 to 3 indicate the different positions of the Au adatoms after adsorption (a) or after their modification while scanning (b) (V=600 mV, I=5 pA, T=77K).

Two additional differences can be noted for Au adatoms. Firstly, once they are adsorbed, Au atoms can be removed during the tip scan. Some of these atoms simply disappear and, in some cases, a characteristic defect due to the deprotonation of the underlying molecule can be observed (Fig. 10). This figure shows the same area before (a) and after (b) two Au atoms were removed from their adsorption site during the tip scan. Once these adatoms have disappeared, the molecular lattice presents the characteristic defect due to TPA deprotonation. From the previous investigations dealing with the apparent corrugation induced by these defects, it appears that the ones observed here correspond to single deprotonation state [30]. This behaviour is not systematic and the adatoms can leave the surface without any modification of the layer. Due to the relative fragility of the self-assembly, the attempts to produce the adatom desorption using voltage pulses without creating other H defects in the vicinity of the original adsorption site never succeeded because of the high electric field induced by the STM tip. In this case, one would be unable to affirm definitively that the defects would be produced by the simple removal of the metallic atoms. These latter are then displaced by the tip while scanning the surface at "low" voltage to be sure that this defect is not produced by the sudden rise of the electric field in the tunneling junction.

Another interesting remark can be made after a precise observation of the Au positions with respect to the TPA network and the chain of molecules (indicated by the black arrow in Fig. 10a). The atoms called 1 have a position already shown in Fig. 8, a position which is the most probable one. Among the remaining atoms, three (named 2) are slightly displaced along the TPA 1D chain, *i.e.* towards the benzene ring of the molecule (and also perpendicularly to the TPA chains but to a less extend). This small displacement along the chain is of about 2 Å in the direction of the TPA chain as compared to the position of the atoms 1. After several tip scans over the same area, two adatoms of type 2 have disappeared and are replaced by two H defects at the same place. Two other adatoms of type 2 present a different contrast and appear now less corrugated. This con-

figuration is named 3. In each case, a small dark contrast can be observed between the remaining protrusions and one of the neighbouring TPA molecules in the same chain. This results indicates that H and induced deprotonated molecules play a significant role in the properties of Au adatoms, either for their adsorption site or concerning their apparent height. This is also highlighted in the Supplementary Informations (Fig. 4) where an STM image obtained several minutes after Fig. 10b shows the creation of numerous defects after desorption of most of the metallic adatoms.

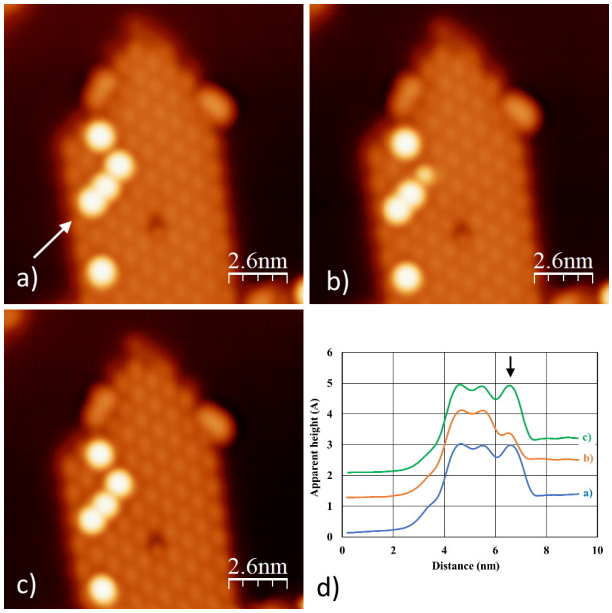

Figure 11: STM images of the same area after modification during the tip scan of one of the adsorbed gold adatoms. (b) has been obtained 4 min after (a) and (c) 49 min after (b). (d) gives the apparent height measured along a line crossing three Au atoms (white arrow) from the Ag(111) lower terrace to the TPA layer. The curves have been vertically displaced for clarity and the black arrow indicates the position of the Au adatom whose contrast changes (V=600mV, I=5 pA, T=77K).

These images suggest that the Au atom contrast may change during the STM experiments. In fact, the contrast modification can be reversible. Fig. 11 presents three STM images of the same area obtained after different scanning times. Starting from an area with five adatoms (Fig. 11a), it is observed that one of these atoms presents a lower contrast after 4 minutes of continuous scan (Fig. 11b). The decrease of this contrast is highlighted in Fig. 11d which shows that the apparent height decreases of 0.7 Å with respect to its original value (see the black arrow). After 49 minutes of scan, the contrast recovers its initial value (Fig. 11c and curve c in Fig. 11d), in good agreement with the other atoms. These modifications are rather difficult to control due to the relative fragility of the molecular layer which prevents to work at high voltage or high tunneling currents, conditions necessary for atomic manipulation. Sometimes, this contrast variation can be followed by the complete desorption of the concerned atom. On single Au atoms deposited on ultrathin layers of NaCl, such contrast modifications have been interpreted in terms of charge deposited on the atoms to form negatively charged species Au^- [43, 44]. For Au on TPA, this interpretation cannot be invoked since the molecular layer is not insulating and the charge cannot be conserved for tens of seconds on a single atom. There is no doubt that Au is "electrically" connected to the metallic substrate and the fact that these observations can also be made for Au adsorbed on two monolayers TPA domains confirms this point. To understand these different observations, DFT calculations have been conducted and are presented in the following paragraphs.

4.5. Calculations for Au atoms on TPA

4.5.1. Different adsorption geometries

With an Au atom, the most stable adsorption position on the TPA ML is just above a carbon atom of the COOH group as indicated in the top panel of Fig. 12 (configuration called "a"). The Au-C distance is 2.112 Å, a value close to that of similar bond length [45]. The adsorption energy is -1.249 eV while the charge transfer leads to a gain of 0.09 electron on the Au adatom and 0.36 electron on the C atom. The adsorption energy shows than Au is less firmly adsorbed than Co (E_{ads}=-4.083 eV for Co adatoms). It should be also noticed that in this configuration, one H atom in the H-bonded dimer is transferred from the TPA on the left to the O atom of the COOH group beneath the Au atom. The number of H atom is then constant but the left molecule is modified by the H transfer. This displacement is indicated by a black curved arrow in Fig. 12, configuration "a". The carboxyl group thus becomes C*OOHH, with an original C=O bond (1.262 Å) stretched to 1.383 Å (C*-O bond). It means a lost of double bond character and the sp2 hybridization of C changed to sp3 for C*. In this configuration, the Au atom is localized at a distance of 1.857 Å to the middle of H-bonded dimer (3.174 Å to the benzene ring center of TPA). This value is in good agreement with the 1.6 Å shift experimentally measured along the TPA chain in Figs. 10. Then, the calculated conformation "a" corresponds to the atoms of type "1" in the STM images.

In addition to the most stable conformation presented above, other Au adsorption positions have been localized on carbon atoms of the benzene ring. For this, the middle panel of Fig. 12 shows another configuration called "b" in which the Au atom binds to the C at the *meta* position. At this position, the Au-C bond length is 2.17 Å and the adsorption energy is -1.06 eV. The C atom to which Au is attached also changes its hybridization from sp2 to sp3. The net charge transfer indicates a gain of 0.15 electron on the Au atom and of 0.18 electron on the C atom, *i.e.* two times smaller than in the "a" conformation. In this case, the H-bonded dimer remains intact. As compared to the previous conformation, the Au atom is then slightly displaced toward the benzene ring along the TPA chain. This displacement is 2.2 Å along the chain and 1.1 Å perpendicularly to the TPA row, values in good agreement with the lateral shift measured in Fig. 10 for the atoms of type "2".

Moreover, the presence of diffusing H atoms on the TPA layer is highly expected. Indeed, it has been demonstrated that the molecular layer suffers from deprotonation as a function of time and that this deprotonation can be simply induced by

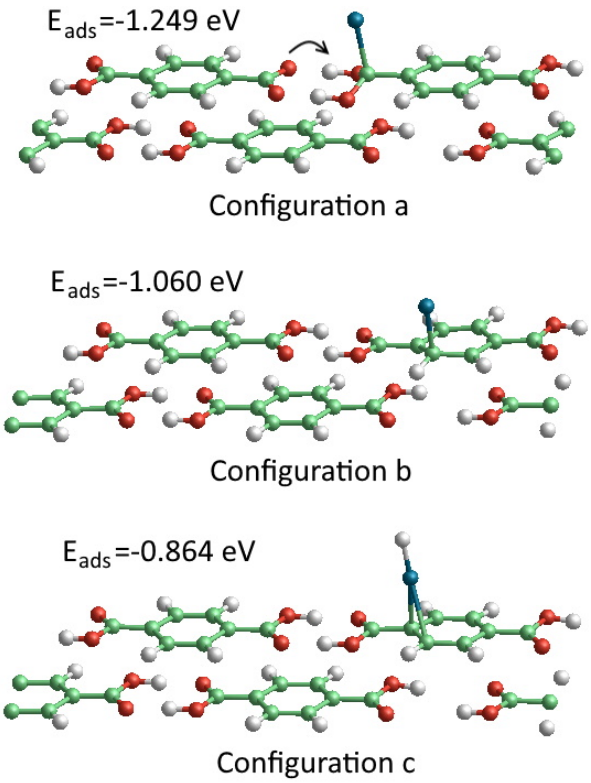

Figure 12: a) DFT calculations showing the most stable conformation with the Au adatom close to the carboxyl group. The adsorption energy is -1.249 eV. The C*-H, C*-O and C*-Au bond lengths are 1.380 Å, 1.383 Å and 2.112 Å respectively. The black arrow shows the motion of the H atom coming from the left molecule. b) Adsorption configuration with the Au atom adsorbed on one of the C atoms of the benzene ring (E_{ad}=-1.060 eV). c) Adsorption of Au-H above a C-C bond of the benzene ring. This conformation presents the lowest adsorption energy (E_{ads}=-0.864 eV).

the STM tip [30]. Diffusion of the so-created "singly deprotonated" defects could be important due to their low activation barrier (typically 0.91 eV). All these arguments suggest that the H atoms could play an important role in the adsorption of metallic adatoms, particularly for Au for which the adsorption energies are significantly smaller than for Co. To mimic such a situation, an extra H atom has been added in the models of "a" and "b" configurations and new calculations have been performed. During the optimization, this supplementary H atom spontaneously attached to the Au atom. In this case, the most stable adsorption site of the thus formed Au-H entity is localized at the middle of one C-C bond on the benzene ring (lower panel of Fig. 12, conformation called "c"). At such a position, the C-Au bond length is about 2.416 Å, with a net charge gain of 0.05 electron on Au and 0.11 electron on the C atom at *para*, while the C atom on *meta* position loses 0.03 electron. The calculated adsorption energy is the smallest with E_{ads}=-0.864 eV.

4.5.2. STM image calculations and role of H atoms

As explained above, three adsorption positions are available and on the other hand, several types of contrasts are experimentally observed. For connecting such experimental observations to the calculated configurations, simulated STM images of the three structures have been calculated according to the Tersoff-Hamann approach [46]. Essentially, these calculations highlight the contribution of the electronic density to the tunneling current whose variations can be related to the observed contrasts.

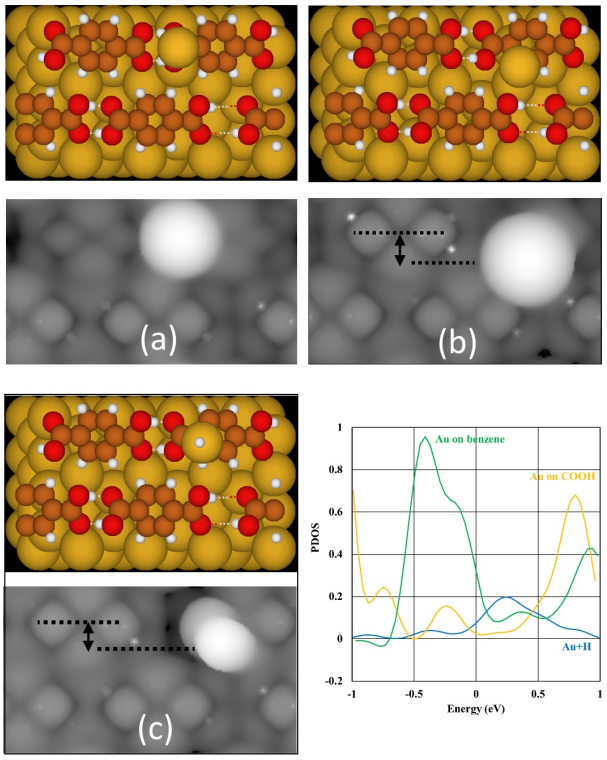

Figure 13: a) Schema showing the most stable conformation with the Au adatom close to the carboxyl group and the calculated STM image using the Tersoff-Hamann approach. b) Conformation with the Au adatom on top of the C at the *meta* position and corresponding calculated STM image. c) Conformation corresponding to (b) but with addition of an H atom on top of Au and corresponding calculated STM image. The double arrows show the shift between the TPA 1D rows and the largest corrugations. d) The curves show the calculated PDOS on the Au atom for this latter in a position in orange, b position in green and with an H atom c in blue.

In the first calculation presented in Fig. 13a and performed from the "a" configuration, the large bump corresponds to the Au adatom close to the H-bond of the TPA dimer. As observed experimentally, this bump has a larger size than a single atom and this is what is generally observed for adatoms This protrusion is perfectly aligned along the TPA row and very similar to the STM image of atom "1" in Fig. 10a. For the second conformation "b", the Au bound to C at *meta* position shows a slightly larger bump (Fig. 13b) which is shifted with respect to the TPA row (indicated by the double black arrow). This calculated image is in good agreement with atom "2" in the experimental STM topography (Fig. 10a). The simulated image of the Au-H

conformation corresponding to the addition of a supplementary H atom is presented in Fig. 13c. Again, this indicates that the bump position is laterally shifted with respect to the molecular row. The calculated image also agrees very well with the experimental contrast of atoms “3” observed in Fig. 10b after the transformation of atoms ”2”. Notably, this transformation resulted in a reduced corrugation of the adatoms in the STM images and this is also the case in the calculations. The Projected Density of States (PDOS) calculated on the Au atom for the three conformations (Fig. 13d) underlines the role of hydrogen. Indeed, these PDOS exhibit a smaller contribution to the electron density for the AuH configuration in an energy range of $\mp$1 eV around the Fermi level. This smaller contribution can explain the decrease of the apparent height experimentally observed as compared to the two previous configurations.

The calculated activation barriers between the configurations ”a” and ”b” (see Fig. 5 in the Supplementary Informations) suggest that these latter can be easily exchanged between them. Moreover, the presence of supplementary H atoms allows for reaching the ”c” conformation. This transformation from ”a” to ”c” or ”b” to ”c” perfectly corresponds to what is observed if Fig. 10b after the transformation of atoms 1 and 2 to the form called 3. Inversely, the loss of a H atom from ”c” allows to return to the ”a” or ”b” configurations as it is observed in Figs. 11 where the same adatom reversibly switches between two states between the three STM images. The attachment and detachment of H atoms on the metallic adatoms then allows to change from a conformation to another. Au adatoms can be also desorbed from the TPA layer. For this, defects have to appear in the molecular layer and this is discussed in the following paragraph.

4.5.3. Role of TPA defects

To illustrate the possible role of deprotonated TPA molecules in the stability of the adatoms, the configuration with an Au atom bound to the C* atom of C*OOHH (Fig. 12, configuration ”a”) is used as a starting point. Remember that in this case, the number of H is conserved and this situation is called no-defective. Thereafter, the H atom initially present on the right TPA (TPA on which the Au is adsorbed) is removed (see Fig. 6 in Supplementary Informations). Finally, one H is missing. As an H atom has been also transferred from the left molecule, this latter is singly deprotonated and this configuration is called L-defective. Moreover, the right TPA supporting the Au adatom has previously received an H from the left one and the C*OOHH becomes again a COOH carboxylic group. In this particular case, the addition of a supplementary hydrogen atom (resulting for example from a distant defect on the TPA layer) firstly leads to the formation of AuH. As a second step however, the adsorbed AuH component is detached from the C to be physisorbed with an adsorption energy of -0.05 eV. In this metastable configuration, the distance from Au to C is stretched to 3.54 Å (*vs* a AuC* bond length of 2.18 Å). Such a lower adsorption energy makes this conformation more rare on the surface and more sensitive to the presence of the STM tip. This could perfectly explain the desorption of Au adatoms experimentally observed during the tip scan (see for example Fig. 10b).

It is also important to study the activation barriers of these mechanisms in order to ensure that they can take place on the surface either by the local electric field between tip and sample or by the injected tunneling electrons. These results are presented in Fig. 14. Thus, even if the attachment of an hydrogen atom on Au does not exhibit any activation energy barrier, the deprotonation starting from the configuration of Au adsorbed on the no-defective TPA requires an activation energy as high as 1.9 eV. An alternative path via an energetically equivalent configuration to the L-defective one has been also identified. In this case, the hydrogen atom on the TPA at the right side of the H-bonded dimer is removed. The singly deprotonated molecule is then the one on which the Au atom is adsorbed. By analogy, this intermediate case is called R-defective configuration. The barrier to transform the R-defective to the L-defective configuration is estimated to 0.9 eV. However, the barrier necessary to pass from the no-defective to these L/R-defective configurations requires at least 1.7 eV.

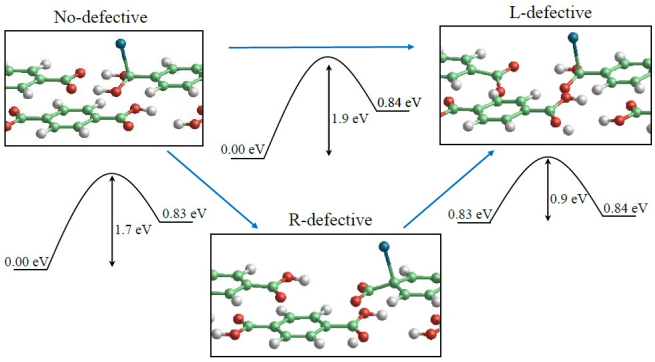

Figure 14: Calculated activation barriers for the L and R defective conformations.

These results show that the calculations performed for the L/R conformations make it possible to test the presence of a singly deprotonated TPA in the concerned H-bounded dimer, the defect being either on the left molecule or on the right one. The difference between L-defective and R-defective is also the adsorption site of the Au adatom. In L-defective, the Au-C bond length is 2.18 Å, and the Au atom has a net charge of +0.13 electron. In R-defective, Au is adsorbed on a singly deprotonated TPA and the completely dehydrogenated carboxylate group strongly binds to the Ag(111) surface through its two oxygen atoms. This induces a migration of the Au atom from the C to the next C1 position of the central benzene ring. The Au-C1 bond length is the same as Au-C, *i.e.* 2.18 Å. Adding a supplementary H atom to the R-defective configuration results in the formation of a stable AuH adsorbed in the middle of a C-C bond as in the case of a no-defective TPA monolayer. Thus, the Au adatoms bounded to an extra H atom can also be stable on the surface if the metallic adatom is adsorbed on a deprotonated TPA. This property is different than for the L defective configuration in which the AuH formed by diffusing hydrogen was highly unstable. Moreover, the higher the *d* states are in

energy relative to Ef, the stronger is the bond between the adsorbate and the transition metal atom [47]. For the R defective configuration, these occupied bands are 0.02 eV closer to the Fermi level than for the L one. This property as well as the presence of the COO carboxylate group could perfectly explain a larger stability of the R situation between the gold atom and the TPA layer while in the L configuration, the Au adatom is more unstable and can be easily desorbed as observed experimentally.

5. SUMMARY

Co and Au atoms have been evaporated on self assembled domains of terephthalic acid molecules. The STM observations and the DFT calculations demonstrate that the two atoms have a different behaviour. Co is firmly bounded to the TPA molecule with an unique adsorption position on top of the benzene ring. Near the Fermi level, a characteristic feature of the electron density due to the metallic atom can be observed in the STS spectra. For Co dimers, calculations demonstrate that the most favoured configuration is obtained when the spins are parallel. Au adatoms have a different behaviour essentially because they present different adsorption sites with lower adsorption energies. They can be adsorbed on top of a C atom of the COOH group or be located on top of a C atom of the benzene ring. The H atoms diffusing on the surface or coming from the surrounding defects in the TPA layer as well as deprotonation of the underlying molecules play an important role in the possible desorption of these adatoms. Their contribution to the electronic density is low and the STS spectra show that the main electronic characteristics of the molecular layer and substrate are quenched by the presence of the metallic adatom.

More generally, these experiments demonstrate that it is possible to make chemistry on single atoms deposited on molecular layers. These latter generally act as host lattices for other molecules but they can also be host structures for single atoms. This opens the way to new experiments in the very promising context of single atom catalysis [48, 49]. Indeed, on such molecular systems, one is able to select the adsorption site as a function of the chosen metallic atom and then produce a model system interacting with a surrounding gas for example. Because adatoms can diffuse on the substrate and be adsorbed on the edge of the molecular domain (for example the Co atoms), it can be possible to organise these adatoms to forms metallic chains. Another interesting point is that this kind of molecular host lattice can be deposited on different substrates such as MoS_2 with exactly the same molecular lattice parameters (Fig. 8 in Supplementary Informations). In this case, this also offers the possibility to investigate the role of deposited adatoms with the semiconducting sub-layers and local charges due to doping.

6. ACKNOWLEDGEMENT

This study has been supported through the EUR grant NanoX n° ANR-17-EURE-0009 in the framework of the "Programme des Investissements d'Avenir".

References

[1] C.A. Mirkin, M. Ratner, Molecular electronics, *Annual Review of Physical Chemistry*, **43(1)** (1992) 719-754.

[2] J.M. Tour, Molecular Electronics. Synthesis and Testing of Components, *Annu. Rev. Phys. Chem.*, **33(11)** (2000) 791-804.

[3] J.M. Lehn, Toward Self-Organization and Complex Matter, *Science*, **295(5564)** (2002) 2400-2403.

[4] J.V. Barth, Molecular Architectonic on Metal Surfaces, *Annu. Rev. Phys. Chem.*, **58** (2007) 375-407.

[5] B. Li, H.M. Wen, Y. Cui, W. Zhou, G. Qian, B. Chen, Banglin, Emerging Multifunctional Metal–Organic Framework Materials, *Adv. Materials*, **28(40)** (2016) 8819-8860.

[6] X.H. Qiu, G.V. Nazin, W. Ho, Mechanisms of Reversible Conformational Transitions in a Single Molecule, *Phys. Rev. Lett.*, **93(19)** (2004)196806-196810.

[7] J.I. Pascual, N. Lorente, Z. Song, H.P. Rust, Selectivity in vibrationally mediated single-molecule chemistry, *Nature*, **423** (2003) 525–528.

[8] P. Liljeroth, I. Swart, S. Paavilainen, J. Repp, G. Meyer, Single-Molecule Synthesis and Characterization of Metal-Ligand Complexes by Low Temperature STM, *Nano Letters*, **10(7)** (2010) 2475-2479.

[9] S. Stepanow, N. Lin, D. Payer, U. Schlickum, F. Klappenberger, G. Zoppellaro, M. Ruben, H. Brune, J.V. Barth, K. Kern, Surface-Assisted Assembly of 2D Metal–Organic Networks That Exhibit Unusual Threefold Coordination Symmetry, *Angewandte Chemie International Edition*, **46(5)** (2007) 710-713.

[10] W. Auwärter, F. Klappenberger, A. Weber-Bargioni, A. Schiffrin, T. Strunskus, C. Wöll, Y. Pennec, A. Riemann, J.V. Barth, Conformational Adaptation and Selective Adatom Capturing of Tetrapyridyl-porphyrin Molecules on a Copper (111) Surface, *Journal of the American Chemical Society*, **129(36)** (2007) 11279-11285.

[11] T. Lin, G. Kuang, X.S. Shang, P.N. Liu, N. Lin, Self-assembly of metal–organic coordination networks using on-surface synthesized ligands, *Chem. Comm.*, **50(97)** (2014) 15327-15329.

[12] L. Grill, M. Dyer, L. Lafferentz, M. Persson, M.V. Peters, S. Hecht, Nano-architectures by covalent assembly of molecular building blocks, *Nature Nanotechnology*, **2** (2007) 687-691.

[13] A. Gourdon, On-Surface Covalent Coupling in Ultrahigh Vacuum, *Angewandte Chemie International Edition*, **47(37)** (2008) 6950-6953.

[14] R. Coratger, B. Calmettes, M. Abel, L. Porte, STM observations of the first polymerization steps between hexahydroxy-tri-phenylene and benzene-di-boronic acid molecules, *Surf. Sci.*, **605(7)** (2011) 831 - 837.

[15] D. Peyrot, F. Silly, On-Surface Synthesis of Two-Dimensional Covalent Organic Structures versus Halogen-Bonded Self-Assembly: Competing Formation of Organic Nanoarchitectures, *ACS Nano*, **10(5)** (2016) 5490-5498.

[16] I. Janica, V. Patroniak, P. Samori, A. Ciesielski, Imine-Based Architectures at Surfaces and Interfaces: From Self-Assembly to Dynamic Covalent Chemistry in 2D, *Chemistry – An Asian Journal*, **13(5)** (2018) 465-481.

[17] T. Ala-Nissila and S.C. Ying, Theory of classical surface diffusion, *Progress in Surface Science*, **39(3)** (1992) 227-323.

[18] D.M. Eigler, E.K. Schweizer, Positioning single atoms with a scanning tunnelling microscope, *Nature*, **344** (1990) 524–526.

[19] S.W. Hla, K.H. Rieder, STM Control of Chemical Reactions: Single-Molecule Synthesis, *Annual Review of Physical Chemistry*, **54(1)** (2003) 307-330.

[20] O. Custance, R. Perez, S. Morita, Atomic force microscopy as a tool for atom manipulation, *Nature Nanotech.*, **4** (2009) 803-810.

[21] S.J.H. Griessl, M. Lackinger,F. Jamitzky, T. Markert, M. Hietschold, W.M. Heckl, Incorporation and Manipulation of Coronene in an Organic Template Structure, *Langmuir*, **20(21)** (2004) 9403-9407.

[22] S. Stepanow, M. Lingenfelder, A. Dmitriev, H. Spillman, E. Delvigne, N. Lin, X. Deng, C. Cai, J.V. Barth, K. Kern, Steering molecular organization and host–guest interactions using two-dimensional nanoporous coordination systems, *Nature Materials*, **3** (2004) 223-233.

[23] B. Calmettes, S. Nagarajan, A. Gourdon, M. Abel, L. Porte, R. Coratger, Bicomponent Supramolecular Packing in Flexible Phthalocyanine Networks, *Angewandte Chemie International Edition*, **47(37)** (2008) 6994-6998.

[24] S. Clair, S. Pons, A.P. Seitsonen, H. Brune, K. Kern, J.V. Barth, STM study of terephthalic Acid Self-Assembly on Au(111): Hydrogen-Bonded

Sheets on an Inhomeneous Substrate, *J. Phys. Chem.*, **108(38)** (2004) 14585-14590.

[25] M.E. Canas-Ventura, F. Klappenberger, S. Clair, S. Pons, K. Kern, H. Brune, T. Strunskus, Ch. Wöll, R. Fasel, J.V. Barth, Coexistence of one- and two-dimensional supramolecular assemblies of terephthalic acid on Pd(111) due to self-limiting deprotonation, *J. Chem. Phys.*, **125(18)** (2006) 184710-184718.

[26] T. Suzuki, T. Lutz, D. Payer, N. Lin, S.L. Tait, G. Costantini, K. Kern, Substrate effect on supramolecular self-assembly: from semiconductors to metals, *Phys. Chem. Chem. Phys.*, **11(30)** (2009) 6498-6504.

[27] M.A. Lingenfelder, H. Spillmann, A. Dmitriev, S. Stepanow, N. Lin, J.V. Barth, Klaus K. Kern, Towards Surface-Supported Supramolecular Architectures: Tailored Coordination Assembly of 1,4-Benzenedicarboxylate and Fe on Cu(100), *Chemistry – A European Journal*, **10(8)** (2004) 1913-1919.

[28] J.D. Fuhr, A. Carrera,N. Murillo-Quirós, L.J. Cristina, A. Cossaro, A. Verdini, L. Floreano, J.E. Gayone, H. Ascolani, Interplay between Hydrogen Bonding and Molecule–Substrate Interactions in the Case of Terephthalic Acid Molecules on Cu(001) Surfaces, *J. Phys. Chem. C*, **117(3)** (2013) 1287-1296.

[29] B. Quiroga-Arganaraz, L.J. Cristina, L.M. Rodriguez, A. Cossaro, A. Verdini, L. Floreano, J.D. Fuhr, J.E. Gayone, H. Ascolani, Ubiquitous deprotonation of terephthalic acid in the self-assembled phases on Cu(100), *Phys. Chem. Chem. Phys.*, **20** (2018) 11552-11560.

[30] J. Heintz, C. Durand, H. Tang, R. Coratger, Control of the deprotonation of terephthalic acid assemblies on Ag(111) studied by DFT calculations and low temperature scanning tunneling microscopy, *Phys. Chem. Chem. Phys.*, **22(6)** (2020) 3173-3183.

[31] G. Kresse, J. Furthmuller, Efficiency of ab-initio total energy calculations for metals and semiconductors using a plane-wave basis set, *Computational Materials Science*, **6(1)** (1996) 0927-0256.

[32] G. Kresse, J. Furthmuller, Efficient iterative schemes for ab initio total-energy calculations using a plane-wave basis set, *Phys. Rev. B*, **6(1)** (1996) 11169-11186.

[33] P. E. Blöchl, Projector augmented-wave method, *Phys. Rev. B*, **50(24)** (1994) 17953-17979.

[34] J.P. Perdew, K. Burke, M. Ernzerhof, Generalized Gradient Approximation Made Simple, *Phys. Rev. Lett.*, **77(18)** (1994) 3865-3868.

[35] S. Grimme, Semiempirical GGA-type density functional constructed with a long-range dispersion correction, *J. of Comput. Chem.*, **27(15)** (2006) 1787-1799.

[36] H.J. Monkhorst, J.D. Pack, Semiempirical GGA-type density functional constructed with a long-range dispersion correction, *Phys. Rev. B*, **13(12)** (1976) 5188-5192.

[37] G. Henkelman, B.P. Uberuaga, J. Hannes, A climbing image nudged elastic band method for finding saddle points and minimum energy paths, *J. Chem. Phys.*, **113(22)** (2000) 9901-9904.

[38] G. Henkelman, J. Hannes, Improved tangent estimate in the nudged elastic band method for finding minimum energy paths and saddle points, *J. Chem. Phys.*, **113(22)** (2000) 9978-9985.

[39] G. Henkelman, J. Hannes, A dimer method for finding saddle points on high dimensional potential surfaces using only first derivatives, *J. Chem. Phys.*, **111(15)** (1999) 7010-7022.

[40] J. Kästner, P. Sherwood, Superlinearly converging dimer method for transition state search, *J. Chem. Phys.*, **128(1)** (2008) 14106-14112.

[41] P. Gambardella, S. Rusponi, M. Veronese, S.S. Dhesi, C. Grazioli, A. Dallmeyer,I. Cabria, R. Zeller, P.H. Dederichs, K. Kern, C. Carbone, H. Brune, Giant Magnetic Anisotropy of Single Cobalt Atoms and Nanoparticles, *J. Chem. Phys.*, **300(5622)** (2003) 1130-1133.

[42] J. Li, W.D. Schneider,R. Berndt, S. Crampin, Electron Confinement to Nanoscale Ag Islands on Ag(111): A Quantitative Study, *Phys. Rev. Lett.*, **(80)15** (1998) 3332-3335.

[43] J. Repp, G. Meyer, F.E. Olsson, M. Persson, Controlling the Charge State of Individual Gold Adatoms, *Science*, **23** (2004) 493-495.

[44] J. Repp, G. Meyer, Scanning tunneling microscopy of adsorbates on insulating films. From the imaging of individual molecular orbitals to the manipulation of the charge state, *Appl. Phys. A*, **85** (2006) 399-406.

[45] A. Antušek, M. Blaško, M. Urban, P. Noga, D. Kisić, M. Nenadović, D. Lončarević, Z. Rakočević, Density functional theory modeling of C–Au chemical bond formation in gold implanted polyethylene, *Phys. Chem. Chem. Phys.*, **19(42)** (2017) 28897-28906.

[46] J. Tersoff, D.R. Hamann, Theory of the scanning tunneling microscope, *Phys. Rev. B*, **31(2)** (1985) 805-813.

[47] J.K. Nørskov, F. Abild-Pedersen, F. Studt, T. Bligaard, Density functional theory in surface chemistry and catalysis, *PNAS*, **108(3)** (2011) 937-943.

[48] G.A. Somorjai, Y. Li, Impact of Surface Chemistry, *PNAS*, **108(3)** (2011) 917-924.

[49] J. Jiao, Y. Wang, H.L. Jiang, Q. Xu, Metal-organic frameworks as platforms for catalytic applications, *Adv. Mater.*, **30** (2018) 1703663-1703686.

Graphical Abstract

Adsorption of single metallic atoms on self-assembled molecular domain of terephthalic acid

Hao Tang, Corentin Durand, Roland Coratger

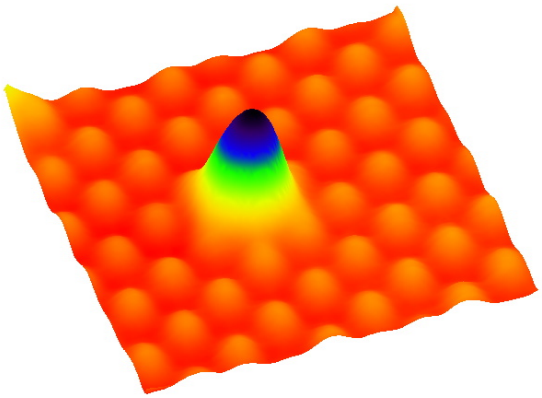

STM image of a Co atom on TPA

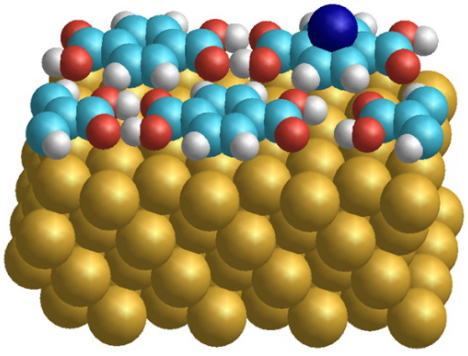

Structure of Co on TPA calculated by DFT